energies

MDPI

Article

Reliability Updating of Offshore Structures Subjected to Marine Growth

Franck Schoefs * and Thanh-Binh Tran

GeM (Institut de Recherche en Génie Civil et Mécanique), Institute for Research in Civil and Mechanical Engineering/IUML (Institut Universitaire Mer et Littoral), Sea and Littoral Research Institute, CNRS UMR 6183/FR 3473, Nantes Université, Ecole Centrale de Nantes, F44322 Nantes, France; binh.tran@univ-nantes.fr

* Correspondence: franck.schoefs@univ-nantes.fr

Abstract: Marine growth is a known problem for oceanic infrastructure and has been shown to negatively impact the reliability of bottom-fixed or floating offshore structures submitted to fatigue or extreme loading. Among other effects, it has been shown to change drag forces by increasing member diameters and modifying the roughness. Bio-colonization being highly random, the objective of this paper is to show how one-site inspection data increases reliability by decreasing uncertainties. This can be introduced in a reliability-based inspection framework for optimizing inspection and maintenance (here, cleaning). The modeling and computation are illustrated through the reliability analysis of a monopile in the European Atlantic area subjected to marine growth and according to the plastic collapse limit state. Based on surveys of structures in the North Sea, long-term stochastic modeling (space and time) of the marine growth thickness is first suggested. A Dynamic Bayesian Network is then developed for reliability updating from the inspection data. Finally, several realistic (10–20 measurements) inspection strategies are compared in terms of reliability improvement and the accuracy of reliability assessment.

Keywords: bio-colonization; Dynamic Bayesian Network; reliability updating; underwater inspection; offshore; monopile

Citation: Schoefs, F.; Tran, T.-B. Reliability Updating of Offshore Structures Subjected to Marine Growth. *Energies* **2022**, *15*, 414. https://doi.org/10.3390/en15020414

Academic Editor: Dimitry Val

Received: 31 October 2021
Accepted: 30 December 2021
Published: 6 January 2022

1. Introduction

Several weeks after immersion, a non-protected offshore structure is covered first by a bio-film and second by macro fouling [1]. Macro fouling acts on the dynamic loading by increasing the mass of the structure, on the hydrodynamics regime by altering the relative roughness [2], on the vibratory response by changing the geometry and mass [3], on drag forces by increasing the diameter of structural members [4–6], and on drag coefficients due to changes in roughness [5,7]. In the Gulf of Guinea, for instance, the thickness of corals up to 25 cm have been reported [8]. This biological phenomenon is affected by the nature (material) and shape of the colonized surface, the age of the structure and the season of installation, the hydrodynamic conditions that affect the fixing and arrival of larvae, the local bio-diversity and the extent of opportunities for colonization and competition [4], and long-term or short-term physio-chemical changes (death or development of the fouling) [8,9]. Understanding this complexity remains challenging because it is site-specific, and it requires on-site measurements of the marine growth with time and the monitoring of environmental parameters. Ongoing projects such as SURFFEOL [10], ABIOP [11], LEHERO-MG [2,12–15], and ABIOP+ [16] attempt to achieve this objective by installing specific buoys [10,17]. Moreover, assessing the evolution of marine growth with time requires accurate non-destructive testing tools in underwater conditions. Recently, the development of specific image processing algorithms is promising [18–20], especially if coupled with underwater drones to increase the safety of divers and reduce costs.

Based on these studies and expanding industry knowledge, the probabilistic modeling (stochastic processes in space and time) of macro fouling appears reachable. Updating models with inspection data for uncertainty reduction is required. Risk-based inspection [21,22] offers a theoretical framework that links reliability, inspection, and risk. This paper focuses on the random effect of marine growth on drag forces and coefficients. It addresses potential significant increases in the screen effect and modifications to the flow regime around oceanic structures.

First, the paper reviews the major effects of marine growth on offshore structures and the key parameters that should be modeled for a structural reliability assessment. Then, a long-term a priori model of growth with time is provided based on observations of an existing database. A Dynamic Bayesian Network is then introduced for modeling the structural reliability and updating marine growth parameters from inspection data. It is built and calibrated from the reliability assessment of a monopile subjected to marine growth. Finally, reliability updating is performed and several inspection strategies are compared on a study case in the North Sea where measurements of marine growth come from real field data.

2. Materials and Methods

2.1. Modeling of Marine Growth Thickness Stochastic Process

Most studies analyzing the hydrodynamic effects of biofouling deal with the behavior of small bodies, usually cylinder components, compared with wavelength; that is the case of offshore monopiles and the components (beams) of offshore jacket structures. Usually, papers aim at modeling the changes in the Morison equation [23]. The present paper is well within this field of modeling. Generally, biofouling has several effects on loading to cylindrical structures and the flow regime. Increasing the diameter of the cylinder is the first direct effect of biofouling on the structural characteristics. The drag and inertia loading on the body are thus modified due to the increase in the projected area, displaced volume, and changes to the hydrodynamic coefficients [4,24]. Furthermore, flow instability will increase along with increases in effective diameter [25]. The second effect reduces the shedding frequency, which directly affects the hydrodynamic loads [4]. Moreover, the growth of biofouling on the structure will increase its structural weight [26]. From a maintenance point of view, biofouling has some negative structural consequences. It obscures the structural surface and needs to be removed prior to any visual inspection or non-destructive testing and maintenance (welding) of the structure by divers or remotely operated vehicles [27]. As another impact, biofouling increases surface roughness. The relative roughness ratio ($e = k/D$, where k is the average peak-to-valley and D is the structure equivalent diameter) from hard biofouling on offshore tubular structures is greater than 10^{-3} and may exceed 10^{-2} [28]. These are significantly higher than those for normal cylinders, which changes the Strouhal number (St) [29,30]. It is worth mentioning that many of the aforementioned studies used surface roughness as an instrument to promote the early transition of the boundary layer in order to simulate high-Reynolds flow phenomena at physically low Reynolds numbers [31–35]. A smaller number of these studies were, in fact, addressing the marine fouling effect.

Marine fouling could be categorized as hard, soft, and long flapping fouling, which have dissimilar consequences. Generally, biofouling in the North Sea is classified into 7 categories: (i) mussels; (ii) kelps; (iii) algae (other than kelps); (iv) barnacles, tubeworms, limpets, etc.; (v) rock borers; (vi) hydroids and bryozoans; and (vii) sponges, anemones, sea squirts, and alcyonium [36]. The biofouling can reach a considerable thickness, with single or multiple layers depending on the site location [8,9]. They grow rapidly in the beginning, but growth tapers off after a few years [8,28].

Bio-colonization is a complex process depending on several environmental variables and biological processes with many interactions between them and with the structural surface [27,37]. The process is so complex it would be unrealistic to envisage a complete model involving a multilayer of various marine organisms that have complex interactions

for survival, growth, and reproduction. Therefore, this paper focuses on the growth of a single dominant species on Atlantic coasts [38,39], the blue mussel Mytilus edulis, which was observed to be in the top three most frequent species. So far, there is neither a long-term model nor a database for the growth of mussels on offshore structures. So, this paper proposes prior stochastic modeling of a mussel's growth with available average and variance values from a sparse, available database of the North Sea and Atlantic coasts. For the modeling of the average thickness trend, a simplified growth model inspired by the model of Bayne [40] and Bayne and Worrall [41] is considered (1). It is derived from more general growth models [42,43] whose application fields have been shown to be various (see the review of Vincenzi et al. [44]). It was shown to be consistent with the average value of a mussel's length S (cm) for the French Atlantic coast [45].

$$S = \alpha\left[1 - e^{-\beta t}\right] \tag{1}$$

where t is the time (in years). The aforementioned equation is used for the modeling of the trend of the average mussel's thickness value. In fact, it is shown [7,8] that the thickness reaches an asymptotic value after about a decade due to several factors: competition, diseases, chocks in environmental conditions, detachment due to storms, or self-weight. A report of Veritec in the North Sea [46] is used in the present paper in view of obtaining a set of experimental data. The measurements of marine growth were reported from the inspection of 18 structures installed between 1970 and 1985. Each structure was inspected 2 or 3 times during this period. The earliest inspection was after 1 year and the latest after 15 years. In absence of a protocol, we know that there is heterogeneity in data collection: the depth of the inspection is reported but not the component or even its orientation (vertical, horizontal, ...). So, for characterizing the prior thickness, the nominal value is defined as the maximum value obtained at a given age between 0 and −10 m depth among the set of structures inspected at this time. Note that this does not mean that it is the maximum value of the process at a given depth, only the maximum value measured in the area of the structure investigated by the diver. In the following, for conservative considerations, this nominal value is considered as the mean value for the model. Table 1 presents the thickness measurements collected after 15 years of inspection. These values are in line with the measurements published for the southern North Sea [47]. Only the maximum measurements at each inspection time are retained for further analysis and it is observed that the marine growth thickness stabilizes at around 40 mm after 10 years. Due to the lack of prior information on a given site, some assumptions about the prior knowledge regarding parameters in (2) (α and β) must be based on available data. In this study, the initial growth velocity is assumed to be equal to 27.5 (mm/year) when the time t reaches 0, according to data obtained from [9]. Hence, prior boundary conditions are established on (2) as follows:

$$Th_{prior}(10) = 40\ (\text{mm}) \tag{2}$$

$$\frac{\partial Th_{prior}}{\partial t}(0) = 27.5\ (\text{mm}) \tag{3}$$

By solving the boundary conditions, we obtain α = 40 and β = 0.6875.

The prior evolution of marine growth thickness is thus given in (3) and plotted in Figure 1. Parameter β in (1) characterizes the evolution trend of a specific mussel and environment. Therefore, in probabilistic modeling, β is considered a constant parameter. Parameter α in (1) represents the magnitude of the thickness of the marine growth. This should be adapted to each site. In this study, α is assumed to be normally distributed with a Coefficient of Variation (COV) equal to 0.3 [4]. Based on these assumptions, the prior mussel's thickness curve Th_{prior} is given in (4) and the evolution of statistics is plotted in Figure 1.

Table 1. Thickness measurements in the North Sea from [46].

	Inspection Time from Installation of Structures (Years)															
	0	**1**	**2**	**3**	**4**	**5**	**6**	**7**	**8**	**9**	**10**	**11**	**12**	**13**	**14**	**15**
Field Measurement (mm)		30	20	20	30	20	10	20	50	40			20	20	10	40
Measurement (mm)		30	70		10	20	40	30	10				20	40	40	40
			50		20	80	30	20					20	20	20	30
					10	10										
					10	20										
					20	30										
						5										
						20										
							30									

$$Th_{ref} = 40\left[1 - e^{-0.6875\,t}\right]\ (\text{mm}) \tag{4}$$

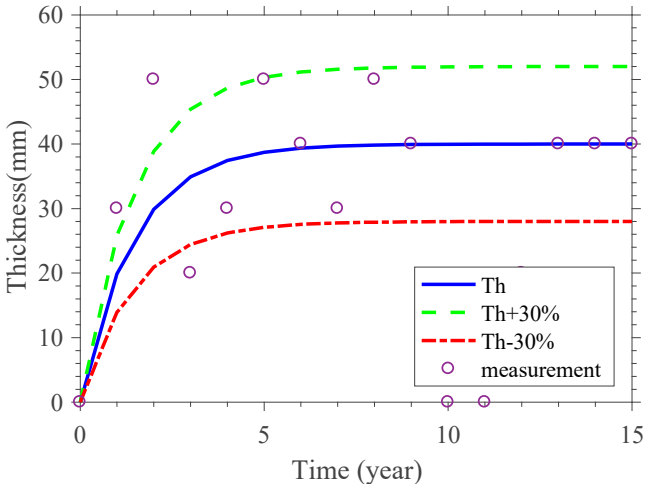

Figure 1. Mussel's thickness evolution based on a database of the North Sea; the blue line represents the mean value trend and the red dashed line represents the mean ± standard deviation.

For structures in other areas, a similar a priori distribution can be exploited from prior thickness on fixed structures or metocean buoys such as Biocolmar® with the same material [48].

2.2. Dynamic Bayesian Networks for Probability Updating

Stochastic loading computation is required for the time-dependent reliability assessment of offshore structures. However, this is time-consuming, especially if changes in the process are observed (inspection cleaning) and because wave loading is a nonlinear process of the random input variables. In this paper, a metamodel is developed for uncertainty propagation in view of reducing the computational costs when implementing several strategies for maintenance. A Bayesian Network (BN) is an efficient approach to graphically modeling the probabilistic dependency between random variables using a directed acyclic graph (DAG). In the DAG, random variables are symbolized by nodes and are connected by edges to illustrate their dependencies. A conditional Probability Density Function (PDF), $f(X \mid \boldsymbol{pa}(X))$ or Probability Mass Function (PMF), $p(X \mid \boldsymbol{pa}(X))$ is assigned to each child node, where $\boldsymbol{pa}(X)$ is the parent of X in the DAG. An edge may represent causal relationships between the variables (nodes), but this is not a requirement. The graphical structure of a BN encodes conditional independence assumptions among the random variables. Hence, a BN is a compact model representing the joint PDF or PMF among random variables. In this

study, only BNs with discrete random variables are considered. The joint PMF of the BN with X_1, X_2, … X_N is formed using the chain rule as:

$$P(X_1, X_2, \ldots, X_N) = \prod_{i=1}^{N} P(X_i | \boldsymbol{pa}(X_i)) \quad (5)$$

where $P(X_i \mid \boldsymbol{pa}(X_i))$ is the conditional PMF of variable X_1 given its parent variables.

Figure 2 illustrates a simple BN that consists of three nodes representing three discrete random variables, X_1, X_2, and X_3, in which X_2 and X_3 are children of the parent node X_1. The joint PMF of the BN present in Figure 2 is expressed as a product of the PMFs of all nodes in the BN:

$$P(X_1, X_2, X_3) = P(X_1)P(X_2|X_1)P(X_3|X_1) \quad (6)$$

where $P(X_i \mid X_j)$ denotes the conditional probability of X_i given X_j.

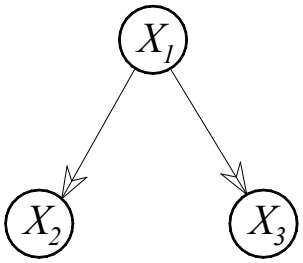

Figure 2. A Simple Bayesian Network.

BNs allow for the introduction of new information (evidence) from the observed nodes (here, inspection data) to update the probabilities in the network. For example, if we have some evidence o to introduce to node X_2 ($X_2 = o$), this information propagates through the network, and the joint PMF of the two other nodes can be recalculated as:

$$P(X_1, X_2, X_3|) = \frac{P(X_1, , X_3)}{P()} = \frac{P(X_1)\mathrm{P}(|X_1)\mathrm{P}(X_3|X_1)}{\sum_{X_1} P(X_1)\mathrm{P}(|X_1)} \quad (7)$$

A DBN is an extended form of a BN, which is often used to present random processes and can be used for modeling a system's performance over its lifetime. Figure 3 presents a simple form of a DBN consisting of T slices. Slices in the DBN are connected by links from nodes in slice $(i-1)$ to nodes in slice i. At each slice is a BN that represents the system performance at that time. The state of the system at slice i depends only on its state in slice $(i-1)$; hence, this DBN could be seen as a Markov Chain. Each slice i of the DBN presented in Figure 3 consists of two nodes, X_i and Y_i, in which their joint probability could be computed as:

$$P(X_i, Y_i) = \sum_{X_{i-1}} P(X_{i-1})P(X_i|X_{i-1})P(Y_i|X_i) \quad (8)$$

where $P(X_{i-1})$ is the marginal probability distribution of node X_{i-1} in slice $(i-1)$, $P(X_i \mid X_{i-1})$ is a transition matrix presenting the conditional probability between the two adjacent slices of node X, and $P(Y_i \mid X_i)$ defines the conditional probability of node Y_i given X_i in slice i.

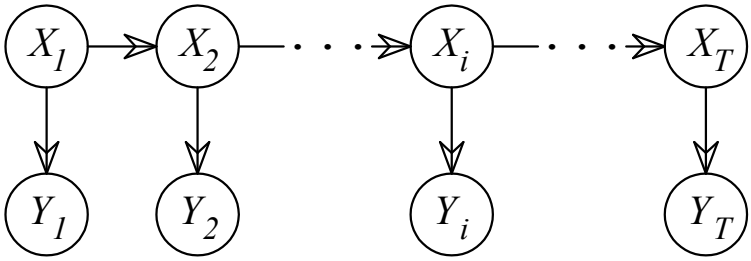

Figure 3. A Dynamic Bayesian Network.

2.3. DBN for Structural Reliability in the Presence of Marine Growth

This section presents how to construct the DBN for reliability modeling and updating the marine growth process. The analysis is performed on a simple structure that is common (81% of grid-connected foundations in Europe in 2019 [49]) in the offshore wind energy industry: the monopile in steel. It is perfectly embedded in the soil and the water depth is 30 m, which is a typical figure for offshore wind turbines (average water depth of online offshore wind farms in 2018 [49]).

Only the wave loading is considered in this paper, as the wind loading is not affected by marine growth; the upper part of the turbine (mast, turbine) is thus not modeled. In view of accounting for the loading of all extreme waves, the total height of the monopile above the soil level is 40 m (Figure 4, left). Moreover, this foundation is shown to be affected by mussels [50,51]; the model presented in Section 2.1 will thus be used. Only one loading case and limit state are considered for this study: the ultimate limit state in the presence of a storm. First, a beam finite element model (BFEM) of a monopile foundation subjected to marine growth colonization was developed (Figure 4, left). Five beams were selected because this was shown to be accurate for representing the loading [52]. A flowchart describing the algorithms for load computation according to Morison equations on the BFEM is presented in Figure 5. The wave loading on the monopile is computed from the well-known Morison equations because the diameter of the monopile is small compared to the wave length [23]. Because the maximum wave load is obtained when the crest of the wave reaches the monopile, only the drag force is considered. The marine growth data is characterized by the growing thickness (*Th*), generated by employing Latin Hypercube simulations in (1). According to the actual knowledge [8,53], a decreasing profile is modeled by using a piecewise-constant model: from 0 to −5 m with the full thickness (4), from 5 to −10 m with half this thickness, and from −10 to bottom without marine growth. Another key parameter [2,7,15] is the roughness of the colonization surface (*k*): this is simulated by using the yearly growth using the gamma process according to [9,54]. The marine growth is assumed to be homogeneous around the pile. As a consequence, the wave is unidirectional (Figure 4 left). The metocean data, represented by a couple of values of significant wave height (*H*) and extreme wave period (*T*), are introduced to calculate the instantaneous flow velocity according to the Airy theory at each node. These values come from the paper by Ameryoun [9] and are derived from the study in [55]. Their joint PDF is plotted in Figure 4 on the right.

Knowing this kinematic field and marine growth, hydraulic parameters (Reynolds *Re* and Keulegan–Carpenter *KC* numbers) are estimated following the procedure already published in [5,52]. The hydrodynamic coefficients (drag coefficient C_D and inertia coefficient C_m), which are useful for modeling the fluid–structure interaction, can then be calculated from these hydraulic parameters.

The output from BFEM is the maximum (at the sea bed) elasticity stress σ, which can be used to define the limit state $g(\boldsymbol{X})$ of the structure, as follows:

$$g(\boldsymbol{X}) = \sigma_e - \sigma \tag{9}$$

where σ_e is the yield stress of the steel and $\boldsymbol{X}$ is the vector of random variables. Table 2 presents the random variables considered in this study: $\boldsymbol{X} = [H; T; \alpha; \beta]$.

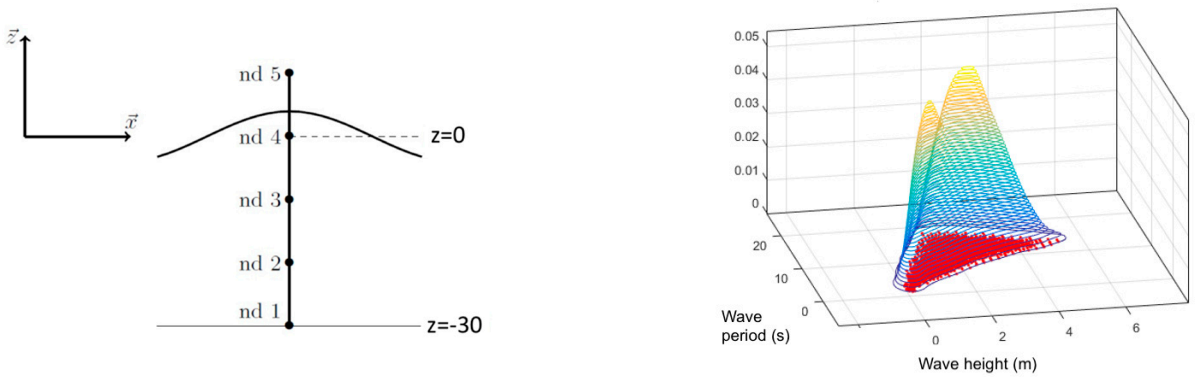

Figure 4. General geometry and finite element model (**left**) and joint PDF of H and T (**right**).

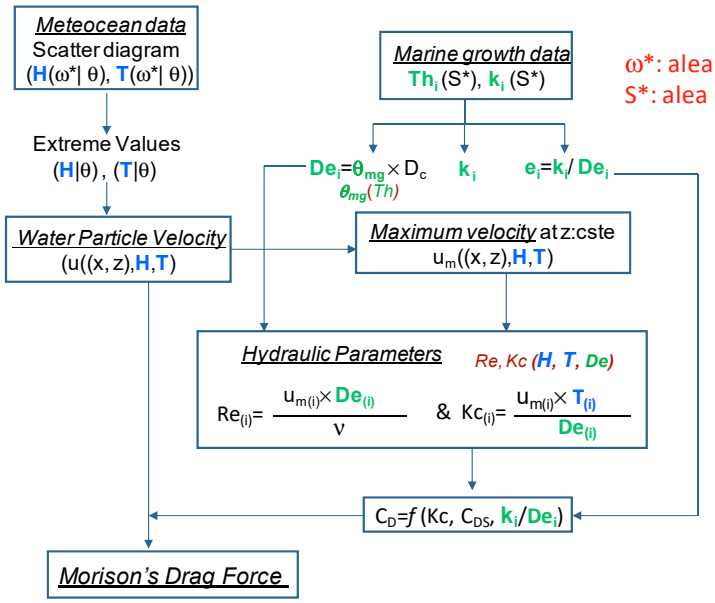

Figure 5. Proposed flowchart for loading computation in the presence of marine growth (adapted from [9]).

Table 2. Input parameters and random variables.

Type	Parameter (Unit)	Description	Value
Geometry and material	D (m)	Diameter	0.3
	d (m)	Water depth (utile length of the monopile)	30
	e (m)	Thickness	0.025
	E (Pa)	Young's modulus	2.1×10^{11}
	G (Pa)	Shear modulus	8.0769×10^{10}
	ρ (kg/m^3)	Density	7800
	σ_e (Pa)	Yield stress	2×10^8
Environment	H and T	See [9]	
Marine growth	α		N(μ = 0.04; COV = 0.3)
	β		0.6875
	Layer 1	From 0 (m) to −5 (m)	$Th_1 = Th$
	Layer 2	From −5 (m) to −19 (m)	$Th_2 = 0.5 \times Th$
	Layer 3	From −10 (m) to bottom (m)	$Th_3 = 0 \times$ Th

For this limit state function, the probability of failure $-P_f$ is determined by integrating the joint density function $f(\boldsymbol{X})$ of the random vector over the failure domain:

$$P_f = P[g(\boldsymbol{X}) \leq 0] = \int\limits_{g(\boldsymbol{X}) \leq 0} f(\boldsymbol{X}) d\boldsymbol{X} \tag{10}$$

Table 2 gathers the input parameters and random variables used for numerical simulations. Uncertainties are propagated throughout the BFEM by generating 30,000 samples based on Latin Hypercube Simulations for each random variable. Data obtained from the BFEM analysis are used to construct the DBN (Figure 6) by computing the Conditional Probability Tables (CPTs) for all nodes in the network. The DBN configuration consists of T slices in which a BN at each slice represents the structural performance at that time. There are 4 nodes in each slice, representing 4 basic random variables: coefficient α, thickness (th), maximum stress (σ), and the limit state (g). The CPTs $P(th_i \mid \alpha_i)$, $P(\sigma_i \mid th_i)$, and $P(g_i \mid \sigma_i)$ define the relationships between parent and child nodes within a slice, and the transition matrices $P(\alpha_i \mid \alpha_{i-1})$ and $P(th_i \mid \alpha_i, th_{i-1})$ describing the dependencies between two neighbor slices are determined from the FEA data. Note that $P(\alpha_i \mid \alpha_{i-1})$ is a unit matrix since α is a time-invariant parameter.

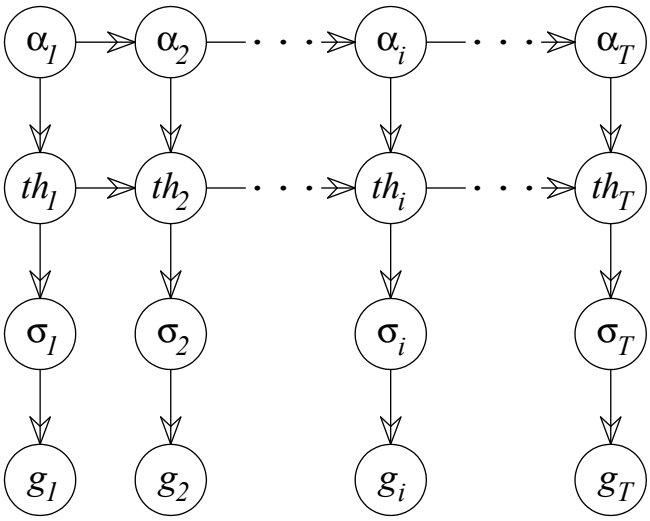

Figure 6. DBN modeling of the marine growth process and limit state assessment.

In this study, we only consider the DBN with discrete nodes; therefore, all nodes are discretized into a number of finite states (Table 3). Each node is divided into a number of states in pre-defined boundaries, which could cover possible values. The discretization of nodes in the DBN could introduce approximation errors [56]; however, this issue is beyond the scope of this study.

Table 3. Discretization of nodes in the DBN.

Nodes	Prior Distribution	Number of States	Boundaries
α	N(μ = 0.04; COV = 0.3)	10	[0; 0.4]
th	-	40	[0; 0.4]
σ	-	40	$[0; 3] \times 10^8$
g	-	Binary	-

3. Results

This section is devoted to performing a reliability assessment of a monopile foundation subjected to marine growth from inspection data, i.e., the measurement of marine growth

thickness (*th*). Numerical measurements are generated from Monte Carlo simulations by assuming that observations are simulated from Equation (4), where α_{obs} follows a normal PDF with mean ${\mu_{obs}}^{\alpha} = 0.027$ and a Coefficient of Variation ${COV_{obs}}^{\alpha} = 0.2$. Note that the mean value and CoV of the observations are selected to be lower than the a priori conservative one. Section 3.1 analyses the effect of the formulation of a limit state, condition-based or performance-based. The Section 3.2 investigates the importance of the number of measurements during an inspection for reliability updating. Then, the following section analyses the effects of combining measurement data from two inspection dates for updating.

3.1. Comparison between Two Limit States

We now assess the reliability by considering two formulations of the ultimate limit state. Considering the limit state based on structural performance, i.e., defined from elasticity stress (9), the prior probability of failure after 25 years, estimated from the DBN, is 1×10^{-3} (Figure 7). Note that reassessment from a structural reliability assessment could be time-consuming and that the stakeholder could be interested in basing their decision-making on a second formulation of the limit state g' relying on the condition state (marine growth thickness). This condition-based limit state writes (11):

$$g'^{(X)} = th_{th} - th \tag{11}$$

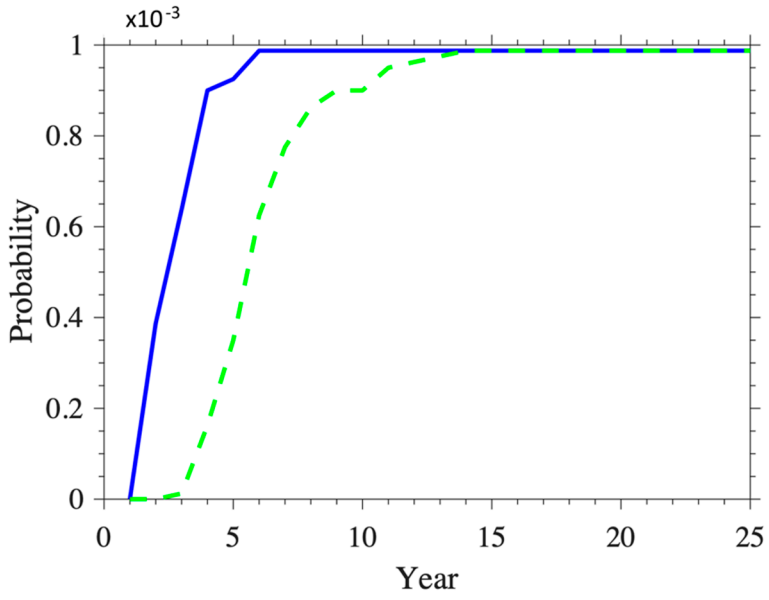

Figure 7. Probability of failure with the two limit states (blue: g; dashed green: g′).

The thickness threshold th_{th} should be defined assuming that an acceptable probability of failure P_{fa} after 25 years is the probability reached by the previous formulation of the limit state: $P_{fa} = 1 \times 10^{-3}$, so the threshold is then $th_{th} = 0.078$ (m). Based on this value, the prior probability of failure defined from this second limit state is computed and reported in Figure 7.

The results in Figure 7 show that, given a similar probability of failure at 25 years, the evolution of P_f computed from the two limit states presents significant discrepancies. At a given time, the prediction of P_f from elasticity stress is higher than the one computed from the thickness measurement. The reliability assessment of structures subjected to marine growth from only thickness measurements is, thus, not sufficiently conservative and a full structural reliability assessment is mandatory. In the following, only limit state (9) is used.

3.2. Reliability Updating from One Inspection Time

Let us focus now on the effect of the number of measurements (evidence) on reliability updating. It is assumed that the first inspection time is performed after the bio-colonization is assumed to be mature, here, five years. This strategy is justified by the fact that an inspection should be carried out neither too early (in the first two years) nor too late in view of capturing the key information about trends and planning preventive maintenance. The assessment considers a typical maintenance ship (mean velocity of 10 knots, https://atlantique-scaphandre.fr/pdf/miniplon.pdf, accessed on 29 December 2021) and a field 30 km from the coast (mean value of bottom-fixed offshore wind-turbines [49]), and 10 h of work, including 3 h of traveling, 2 h of deployment and retrieval, and a 5 h dive. Due to the diving time restrictions, it is assumed that a single diver is carrying out the measurements at a given time. That means that about 20 measurements can be performed (four components per hour). This figure corresponds to the actual practice of the stakeholders [8,46]. First, the reliability updating from 20 measurements is analyzed; these are used as evidence for the DBN update. The updating being affected by the statistical distribution of these 20 measurements, 1000 inspection data are simulated. Figure 8 (left) presents the prior probability of failure and the mean and 95% and 5% quantiles for the updated probability of failure P_f with limit state g (9).

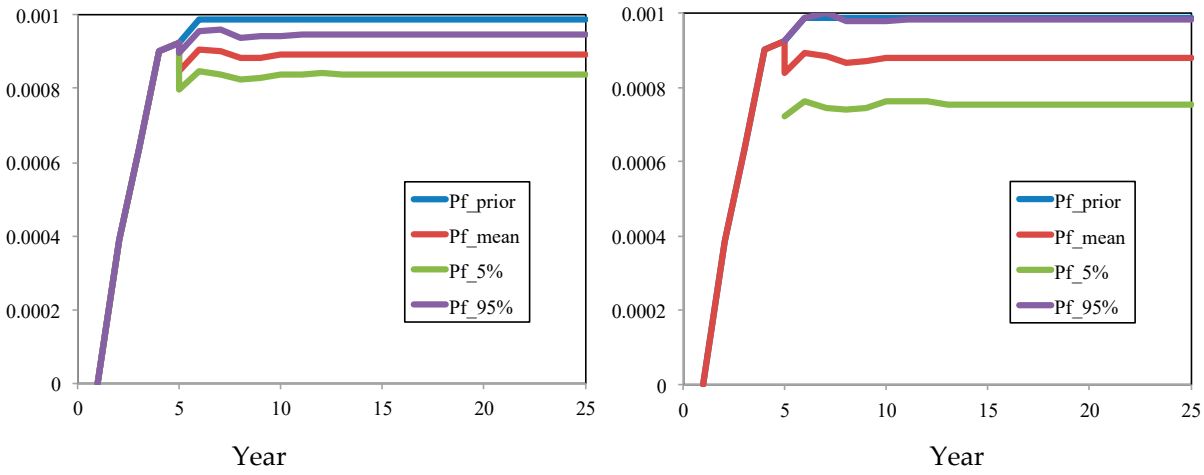

Figure 8. Updated probability of failure with: (**left**) 20 inspection data at 5 years and (**right**) 5 inspection data after 5 years.

The extent of observed marine growth is smaller on average than that which was a priori in (4). Thus, the mean of P_f is smaller with a difference of 1×10^{-4}, i.e., 10% of P_{fa}. It is interesting to underline that the difference between 5% and 95% quantiles and the mean trend P_f (Pf-mean in Figure 8) is not significant and reaches 1×10^{-4}, i.e., 12% of P_f. Twenty measurements appear to give a good update with good accuracy on P_f.

Bayesian updating is influenced by the amount of available evidence. Let us now analyze the effect of the number of measurements. In Figure 8, right, P_f is updated when only five measurements are taken at 5 years. It is clear that when fewer measurements are available, the gap between 5% and 95% of the posterior of P_f increases, reaching 17×10^{-5}, i.e., 20% compared to P_f, and even the interest of the updating is questionable: the 5% fractile is 7.6×10^{-4}. By varying the number of measurements for updating between 3 and 100, Figure 9 presents different quantiles of the posterior of P_f at 5 years with a convergence trend when the number of measurements increases. Table 4 presents the relative errors computed with 5% and 95% with respect to the mean value of P_f. In real practice, the structure owners require the minimization of the number of measurements in order to reduce inspection costs. For offshore structures, due to the high cost of transportation, labor, and hired vessels, 20 measurements appear to be a good compromise with an error in the assessment of P_f of less than 6%, which could be an acceptable error level (Table 4).

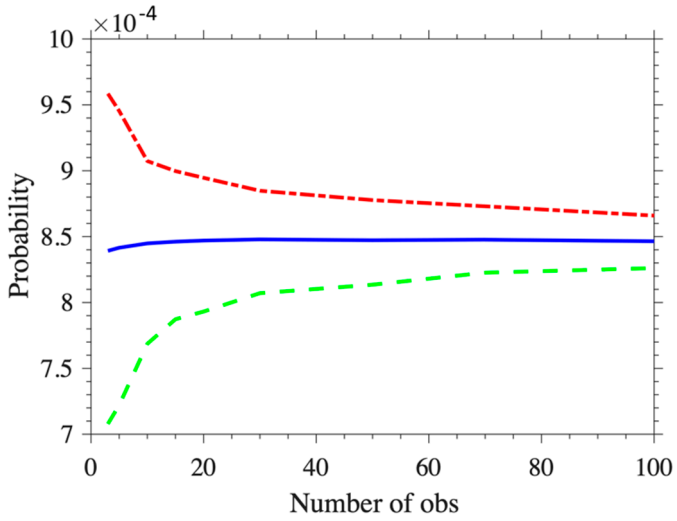

Figure 9. Mean, 5% and 95% confidence interval of the updated probability of failure at 5 years.

Table 4. Errors of 5% and 95% fractiles of P_f with different numbers of simulated inspection data.

	Errors Relative to Mean P_f								
No of Measurement	**3**	**5**	**10**	**15**	**20**	**30**	**50**	**70**	**100**
5% quantiles	16%	14%	9%	7%	6%	5%	4%	3%	2%
95% quantiles	14%	12%	7%	6%	6%	4%	4%	3%	2%

3.3. Reliability Updating from Two Inspection Dates

This section studies the effect of combining measurements from two inspection dates for reliability assessment. The objective of such an analysis is to study the efficiency of different inspection campaigns.

The same budget is defined for each strategy in terms of the number of measurements: 20 total measurements, which could be conducted either 5 or 10 years after the structure's installation (for example, 10 at 5 years and 10 at 10 years equals 20 total inspection data). Three inspection schedules are considered, as shown in Table 5. Figure 10 presents the updating of P_f for each of these schedules. Note that the hidden value of P_f, which is calculated from the assumed value of α (${\mu_{obs}}^{\alpha}$ = 0.027 and ${COV_{obs}}^{\alpha}$ = 0.2), is also plotted in Figure 10. The P_f updated in three cases is lower than its prior one because of the lower mean assumption of α_obs. However, there are significant differences between the updated values of P_f and their hidden values. This trend could be explained by the fact that the thickness measurements for the prior model were not categorized in horizontal and vertical components. This limitation leads to important differences between the updated and hidden values of P_f. By using evidence from the measurements from two inspection dates (case 2), the mean of the updated probability of failure is lower than those in the case of using measurements from only one inspection time (case 1 and case 3) (Figure 10). This behavior highlights the importance of having more inspection dates during the service life of structures to obtain better predictions.

Table 5. Analysis cases with 2 possible inspection dates and a total of 20 inspection data during the service lifetime.

Case	**Number of Measurements**	
	5 Years	**10 Years**
1	20	0
2	10	10
3	0	20

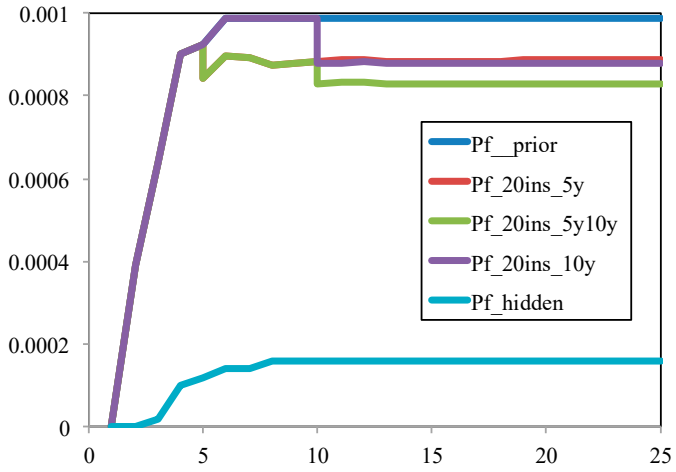

Figure 10. Updated probability of failure with 20 inspections and different inspection dates.

4. Discussion

Marine growth is experiencing a renewed interest in the reliability assessment of existing offshore wind turbines or the optimization of the maintenance of these turbines. This phenomenon being stochastic, this paper has proposed a long-term evolution of thicknesses based on the literature and some available data for the bio-colonization of mussels which is one of the dominant species in the North Sea and on the European Atlantic Coasts. Until now, the link between the long-term modeling of the marine growth, its effect on the structural reliability, and the updating from inspections have not been investigated. This paper offers a complete framework and illustrates its interest with three studies: the effects of the limit state formulation, updating with one inspection, and updating with two inspections with a limited budget along the service lifetime.

If the conclusions are site-specific, the paper provides an efficient framework for updating marine growth evolution with time that can be used at other sites. This approach can thus be transferred to other sites once the extreme values of marine growth are known. This highlights the need for on-site observatories and the share of knowledge through open science and open databases.

5. Conclusions

The paper focuses on an efficient structural reliability updating based on a Dynamic Bayesian Network to update the probability of failure with evidence (measurements) of marine growth. This network is built and calibrated on the basis of a structural finite element model of a monopile where the loading integrates, through the Morison equation, the marine growth effect on both the diameter and the change in hydrodynamical coefficients.

A real study case is then analyzed, using real data from the North Sea. Two limit states, one based on a performance criterion and assessed through full structural reliability and the second based on a condition assessment, are first compared. It was shown that the condition assessment is not sufficiently conservative and cannot be considered as a criterion for decision making (cleaning).

Then, several strategies for the inspection of marine growth thicknesses are compared with single or double inspection times. It was shown that, given a fixed budget for inspection, two inspection dates at 5 and 10 years can sufficiently improve reliability updating.

The key input required for using this framework is a long-term model of marine growth thickness. This paper provides, on the basis of some preliminary data and biological knowledge, a long-term stochastic model of thickness increase with time.

Future studies should integrate a cleaning strategy with more or less efficient cleaning methods.

Author Contributions: Conceptualization, F.S.; methodology, F.S., T.-B.T.; validation, F.S.; formal analysis, F.S.; writing—original draft preparation, T.-B.T.; writing—review and editing, F.S.; project administration, F.S. All authors have read and agreed to the published version of the manuscript.

Funding: This research was funded by COSELMAR (2012–2016) and SURFFEOL (2014–2018).

Data Availability Statement: Not applicable.

Acknowledgments: The authors acknowledge the Sea and Littoral Research Institute (www.iuml-cnrs.fr, accessed on 29 December 2021) for supporting the initiation of work and Région Pays de la Loire for the opportunity to advance the work in the COSELMAR (2012–2016) and SURFFEOL (2014–2018) projects. The authors are grateful to Hamed Ameryoun for preparing the numerical database and to Chantiers de l'Atlantique for leading the SURFFEOL project.

Conflicts of Interest: The authors declare no conflict of interest.

References

1. Characklis, W.G.; Marshall, K.C. Microbial fouling and microbial biofouling control. In *Biofilms*; Characklis, W.G., Marshall, K.C., Eds.; John Wiley and Sons Inc.: New York, NY, USA, 1990; pp. 523–634.
2. Marty, A.; Schoefs, F.; Soulard, T.; Berhault, C.; Facq, J.-V.; Gaurier, B.; Germain, G. Effect of Roughness of Mussels on Cylinder Forces from a Realistic Shape Modelling. *J. Mar. Sci. Eng.* **2021**, *9*, 598. [CrossRef]
3. Zeinoddini, M.; Bakhtiari, A.; Schoefs, F.; Zandi, A.P. Towards an understanding of marine fouling effects on the vortex-induced vibrations of circular cylinders: Partial coverage issue. *Biofouling* **2017**, *33*, 268–280. [CrossRef]
4. Jusoh, I.; Wolfram, J. Effects of marine growth and hydrodynamic loading on offshore structures. *J. Mek.* **1996**, *1*, 77–98.
5. Schoefs, F.; Boukinda, M.L. Sensitivity Approach for Modeling Stochastic Field of Keulegan–Carpenter and Reynolds Numbers Through a Matrix Response Surface. *J. Offshore Mech. Arct. Eng.* **2010**, *132*, 011602. [CrossRef]
6. Wolfram, J.; Jusoh, I.; Sell, D. Uncertainty in the Estimation of Fluid Loading Due to the Effects of Marine Growth. In Proceedings of the 12th International Conference on Offshore Mechanical and Arctic Engineering (OMAE 1993), Glasgow, Scotland, 20–24 June 1993; Volume 2, pp. 219–228.
7. Theophanatos, A. Marine Growth and the Hydrodynamic Loading of Offshore Structures. Ph.D. Thesis, University of Srathclyde, Glasgow, UK, 1988.
8. Mbadinga, M.L.B.; Schoefs, F.; Quiniou-Ramus, V.; Birades, M.; Garretta, R. Marine Growth Colonization Process in Guinea Gulf: Data Analysis. *J. Offshore Mech. Arct. Eng.* **2007**, *129*, 97–106. [CrossRef]
9. Ameryoun, H.; Schoefs, F.; Barillé, L.; Thomas, Y. Stochastic Modeling of Forces on Jacket-Type Offshore Structures Colonized by Marine Growth. *J. Mar. Sci. Eng.* **2019**, *7*, 158. [CrossRef]
10. Schoefs, F.; Ameryoun, A. On-site test of components and sensors exposed to marine degradations processes: Fatigue, corrosion and biofouling. In Proceedings of the 3rd Offshore Wind R&D Conference, Topic Test Facilities & Demonstration Sites, Atlantic Sail City Hotel, Bremerhaven, Germany, 14–16 November 2018; Available online: https://www.rave-offshore.de/en/conference-2018.html (accessed on 29 December 2021).
11. Quillien, N.; Ameryoun, H.; Barillier, A.; Berhault, C.; Boukerma, K.; Bressy, C.; Briand, J.F.; Cayocca, K.; Compère, C.; Damblans, G.; et al. Biofouling: The need to develop interdiscisplinary teamwork skills for MRE. In Proceedings of the International Conference on Ocean Energy (ICOE 2018), Session Underwater Technologies Getting Wet, Corroded and Colonized, La Cité de la Mer, Cherbourg, France, 12–14 June 2018.
12. Bakhtiari, A.; Schoefs, F.; Ameryoun, H. Unified Approach For Estimating Of The Drag Coefficient In Offshore Structures In Presence Of Bio-Colonization. In Proceedings of the 37th International Conference on Offshore Mechanics and Arctic Engineering (O.M.A.E.' 18), Madrid, Spain, 17–22 June 2018.
13. Schoefs, F.; Bakhtiari, A.; Hameryoun, H.; Quillien, N.; Damblans, G.; Reynaud, M.; Berhault, C.; O'Byrne, M. Assessing and modeling the thickness and roughness of marine growth for load computation on mooring lines. In Proceedings of the Floating Offshore Wind Turbine Conference (FOWT 2019), Session Friday Morning 'Wind Energy Devices I', Le Corum, Montpellier, France, 24–26 April 2019.
14. Schoefs, F.; O'Byrne, M.; Pakrashi, V.; Gosh, B.; Oumouni, M.; Soulard, T.; Reynaud, M. Fractal Dimension as an Effective Feature for Characterizing Hard Marine Growth Roughness from Underwater Image Processing in Controlled and Uncontrolled Image Environments. *J. Mar. Sci. Eng.* **2021**, *9*, 1344. [CrossRef]
15. Marty, A.; Berhault, C.; Damblans, G.; Facq, J.-V.; Gaurier, B.; Germain, G.; Soulard, T.; Schoefs, F. Experimental study of hard marine growth effect on the hydrodynamical behaviour of a submarine cable. *Appl. Ocean Res.* **2021**, *114*, 102810. [CrossRef]
16. Quillien, N.; Damblans, G.; Boukerma, K.; Briand, J.F.; Bressy, C.; Carlier, A.; Compère, C.; Dreanno, C.; Jacob, D.; Leblanc, V.; et al. Why and how characterizing biofouling for FOWT? In Proceedings of the Floating Offshore Wind Turbine Conference (FOWT 2019), Session Friday Afternoon 'Resource and Environmental Impact', Le Corum, Montpellier, France, 24–26 April 2019.
17. Schoefs, F.; Chapeleau, X.; Lupi, C. Statistical analysis of Mooring loading of a buoy through FOS and use in risk analysis. In Proceedings of the 54th ESReDA Seminar on Risk, Reliability and Safety of Energy Systems in Coastal and Marine Environments, Université de Nantes, Sea and Litoral Research Institute, MSH Ange Guepin, Nantes, France, 25–26 April 2018.

18. O'Byrne, M.; Schoefs, F.; Pakrashi, V.; Ghosh, B. An underwater lighting and turbidity image repository for analysing the performance of image-based non-destructive techniques. *Struct. Infrastruct. Eng.* **2017**, *14*, 104–123. [CrossRef]
19. O'Byrne, M.; Pakrashi, V.; Schoefs, F.; Ghosh, B. A Stereo-Matching Technique for Recovering 3D Information from Underwater Inspection Imagery. *Comput. Civ. Infrastruct. Eng.* **2018**, *33*, 193–208. [CrossRef]
20. O'Byrne, M.; Pakrashi, V.; Schoefs, F.; Ghosh, B. Semantic Segmentation of Underwater Imagery Using Deep Networks Trained on Synthetic Imagery. *J. Mar. Sci. Eng.* **2018**, *6*, 93. [CrossRef]
21. Faber, M.H.; Hansen, P.F.; Jepsen, F.D.; Mo/ller, H.H. Reliability-Based Management of Marine Fouling. *J. Offshore Mech. Arct. Eng.* **2001**, *123*, 76–83. [CrossRef]
22. Rouhan, A.; Schoefs, F. Probabilistic modeling of inspection results for offshore structures. *Struct. Saf.* **2003**, *25*, 379–399. [CrossRef]
23. Morison, J.R.; Johnson, J.W.; Schaaf, S.A. The Force Exerted by Surface Waves on Piles. *J. Pet. Technol.* **1950**, *2*, 149–154. [CrossRef]
24. Yan, T.; Yan, W.; Dong, Y.; Wang, H.; Yan, Y.; Liang, G. Marine fouling of offshore installations in the northern Beibu Gulf of China. *Int. Biodeterior. Biodegrad.* **2006**, *58*, 99–105. [CrossRef]
25. Henry, P.-Y.; Nedrebø, E.L.; Myrhaug, D. Visualisation of the effect of different types of marine growth on cylinders' wake structure in low Re steady flows. *Ocean Eng.* **2016**, *115*, 182–188. [CrossRef]
26. Shi, W.; Park, H.-C.; Baek, J.-H.; Kim, C.-W.; Kim, Y.-C.; Shin, H.-K. Study on the marine growth effect on the dynamic response of offshore wind turbines. *Int. J. Precis. Eng. Manuf.* **2012**, *13*, 1167–1176. [CrossRef]
27. Dürr, S.; Thomason, J.C. *Biofouling*; Wiley-Blackwell: New York, NY, USA, 2009; Available online: http://eu.wiley.com/WileyCDA/WileyTitle/productCd-1405169265.html (accessed on 29 December 2021).
28. API RP 2A WSD. *Recommended Practice for Planning, Designing, and Constructing Fixed Offshore Platforms*, 21st ed.; API Publications Department: Washington, District of Columbia, United States, 2005; Volume 2.
29. Sarpkaya, T. On the Effect of Roughness on Cylinders. *J. Offshore Mech. Arct. Eng.* **1990**, *112*, 334–340. [CrossRef]
30. Buresti, G. The effect of surface roughness on the flow regime around circular cylinders. *J. Wind. Eng. Ind. Aerodyn.* **1981**, *8*, 105–114. [CrossRef]
31. Batham, J.P. Pressure distributions on circular cylinders at critical Reynolds numbers. *J. Fluid Mech.* **1973**, *57*, 209–228. [CrossRef]
32. Güven, O.; Farell, C.; Patel, V.C. Surface-roughness effects on the mean flow past circular cylinders. *J. Fluid Mech.* **1980**, *98*, 673–701. [CrossRef]
33. Ribeiro, J.D. Effects of surface roughness on the two-dimensional flow past circular cylinders I: Mean forces and pressures. *J. Wind. Eng. Ind. Aerodyn.* **1991**, *37*, 299–309. [CrossRef]
34. Ribeiro, J.D. Effects of surface roughness on the two-dimensional flow past circular cylinders II: Fluctuating forces and pressures. *J. Wind. Eng. Ind. Aerodyn.* **1991**, *37*, 311–326. [CrossRef]
35. Zhou, B.; Wang, X.; Gho, W.M.; Tan, S.K. Force and flow characteristics of a circular cylinder with uniform surface roughness at subcritical Reynolds numbers. *Appl. Ocean Res.* **2015**, *49*, 20–26. [CrossRef]
36. Callow, M.E.; Callow, J.A. Marine biofouling: A sticky problem. *Biologist* **2002**, *49*, 1–5.
37. Railkin, A.I. *Marine Biofouling: Colonization Processes and Defenses*; CRC Press: Boca Raton, FL, USA, 2003.
38. Handå, A.; Alver, M.; Edvardsen, C.V.; Halstensen, S.; Olsen, A.J.; Øie, G.; Reitan, K.I.; Olsen, Y.; Reinertsen, H. Growth of farmed blue mussels (*Mytilus edulis* L.) in a Norwegian coastal area; Comparison of food proxies by DEB modeling. *J. Sea Res.* **2011**, *66*, 297–307. [CrossRef]
39. Heaf, N.J. The Effect of Marine Growth on the Performance of Fixed Offshore Platforms in the North Sea. In Proceedings of the Offshore Technology Conference, Houston, TX, USA, 30 April–3 May 1979; p. 14. [CrossRef]
40. Bayne, B.L. Growth and the delay of metamorphosis of the larvae of *Mytilus edulis* (L.). *Ophelia* **1965**, *2*, 1–47. [CrossRef]
41. Bayne, B.L.; Worrall, C.M. Growth and Production of Mussels Mytilus edulis from Two Populations. *Mar. Ecol. Prog. Ser.* **1980**, *3*, 317–328. [CrossRef]
42. Gompertz, B., XXIV. On the nature of the function expressive of the law of human mortality, and on a new mode of determining the value of life contingencies. In a letter to Francis Baily, Esq. FRS &c. *Philos. Trans. R. Soc. Lond.* **1825**, *115*, 513–583. [CrossRef]
43. von Bertalanffy, L. Quantitative Laws in Metabolism and Growth. *Q. Rev. Biol.* **1957**, *32*, 217–231. [CrossRef]
44. Vincenzi, S.; Jesensek, D.; Crivelli, A.J. Biological and statistical interpretation of size-at-age, mixed-effects models of growth. *R. Soc. Open Sci.* **2020**, *7*, 192146. [CrossRef] [PubMed]
45. Barillé Boyer, A.-L. Contribution à l'étude des potentialités conchylicoles du Pertuis Breton. Ph.D. Thesis, Université d'aix Marseille, Marseille, France, 1996. (In French).
46. Veritec. *Marine Growth Data Bank-Volume 3*; Final report of JIP "MAGDA", Internal Report of Veritec; Veritec: Minneapolis, MN, USA, 1987.
47. van der Stap, T.; Coolen, J.W.P.; Lindeboom, H.J. Data from: Marine fouling assemblages on offshore gas platforms in the southern North Sea: Effects of depth and distance from shore on biodiversity. *PLoS ONE* **2016**, *11*, e0146324. [CrossRef]
48. Decurey, B.; Schoefs, F.; Barillé, A.-L.; Soulard, T. Model of Bio-Colonisation on Mooring Lines: Updating Strategy Based on a Static Qualifying Sea State for Floating Wind Turbines. *J. Mar. Sci. Eng.* **2020**, *8*, 108. [CrossRef]
49. Komušanac, I. *Wind Energy in Europe in 2019: Trends and Statistics*. On Line Resource. Published in February 2020. Available online: https://windeurope.org (accessed on 29 December 2021).

50. Maar, M.; Bolding, K.; Petersen, J.K.; Hansen, J.L.; Timmermann, K. Local effects of blue mussels around turbine foundations in an ecosystem model of Nysted off-shore wind farm, Denmark. *J. Sea Res.* **2009**, *62*, 159–174. [CrossRef]
51. Bruijs, M.C.M. *Biological Fouling Survey of Marine Fouling on Turbine Support Structures of the Offshore784Windfarm Egmond aan Zee*; Report prepared for Noordzeewind; 50863511-TOS/PCW 10-4207,785 OWEZ_R_112_T1_20100226; KEMA Nederland B.V.: Arnhem, The Netherlands, 2010.
52. Schoefs, F. Sensitivity approach for modelling the environmental loading of marine structures through a matrix response surface. *Reliab. Eng. Syst. Saf.* **2008**, *93*, 1004–1017. [CrossRef]
53. Picken, G.B. Review of marine fouling organisms in the North Sea on offshore structures. In *Discussion Forum and Exhibition on Offshore Engineering with Elastomers*; Plastics and Rubber Inst.: London, UK, 1985; Volume 5, pp. 5.1–5.10.
54. El Hajj, B.; Schoefs, F.; Castanier, B.; Yeung, T. A condition-based deterioration model for the stochastic dependency of corrosion rate and crack propagation in a submerged concrete structure. *Comput. Aided Civ. Infrastruct. Eng.* **2016**, *32*, 18–33. [CrossRef]
55. Nerzic, R.; Frelin, C.; Prevosto, M.; Quiniou-Ramus, V. Joint Distributions for Wind/waves/current in West Africa and derivation of Multi Variate Extreme I-FORM Contours. In Proceedings of the 17th International Offshore and Polar Engineering Conference, Lisbon, Portugal, 1–6 July 2007; pp. 81–88.
56. Straub, D. Stochastic Modeling of Deterioration Processes through Dynamic Bayesian Networks. *J. Eng. Mech.* **2009**, *135*, 1089–1099. [CrossRef]